

Flexural buckling behaviour and resistances of circular high strength concrete-filled stainless steel tube columns



An He^a, Yating Liang^b, Ou Zhao^{a,*}

^a School of Civil and Environmental Engineering, Nanyang Technological University, Singapore

^b School of Engineering, University of Glasgow, Glasgow, UK

ARTICLE INFO

Keywords:

Circular high strength concrete-filled stainless steel tube column
End shortening and lateral deflection
Flexural buckling
Initial global geometric imperfection measurements
International design codes
Longitudinal strains
Material testing
Numerical modelling
Pin-ended column tests

ABSTRACT

The flexural buckling behaviour and resistances of circular high strength concrete-filled stainless steel tube (HCSST) columns were examined based on experiments and numerical modelling, and reported in the present paper. The experimental programme was conducted on 12 circular HCSST columns with various member relative slendernesses, and included material tests, initial global geometric imperfection measurements and pin-ended column tests, with their procedures and setups fully described. The experimentally observed results, including the failure loads and modes as well as the load-deformation curves (load-end shortening curves and load-mid-height lateral deflection curves) of the circular HCSST column specimens and the development of the longitudinal strains of the outer stainless steel tubes, were presented and discussed. The experimental programme was then supplemented by a numerical modelling programme, where finite element models were developed and validated against the test results, and then used for conducting parametric studies to generate further numerical data on circular HCSST columns over a broad spectrum of cross-section dimensions and member lengths. Owing to the lack of international design codes for stainless steel–high strength concrete composite structures, the relevant codified design rules for circular normal strength concrete-filled carbon steel tube columns failing by flexural buckling, as used in Europe, America and Australia/New Zealand, were assessed for their applicability to circular HCSST columns, based on the obtained experimental and numerical data. The assessment results indicated that the design rules, as given in the Australian/New Zealand standard and American specification, lead to many unsafe flexural buckling resistance predictions when used for circular HCSST columns, while the design rules, as adopted in the European code, result in more safe and reliable design resistances for circular HCSST columns failing by flexural buckling.

1. Introduction

Circular concrete-filled steel tube (CFST) columns are widely adopted in high-rise buildings and long-span bridges, owing to the (i) superior load-carrying capacities and (ii) low drag coefficients when exposure to fluid and wind. In recent years, circular CFST columns with the outer tubes made of stainless steel have been gaining popularity in civil engineering, as stainless steel possesses more advantageous material properties, including high strength, exceptional ductility and excellent corrosion resistance, than normal carbon steel [1]. The distinct structural behaviour of circular concrete-filled stainless steel tube (CFSST) columns also attracts attention from researchers, with previous studies briefly reviewed herein. At cross-sectional level, the behaviour and resistances of circular CFSST stub columns under concentric [2–4] and eccentric [3] compression were examined, based on a series of

tests; the circular CFSST stub columns were found to exhibit more ductile structural behaviour than their counterparts with the outer tubes made of normal carbon steel. Comparisons of the test failure loads with the codified resistance predictions [2–4] revealed that the codified design rules, originally developed for circular concrete-filled carbon steel tube stub columns, may not be applicable to circular CFSST stub columns, and revised slenderness limits specific for classification of circular CFSST cross-sections were then proposed by Azad et al. [4]. Innovative construction materials, including seawater and sea sand concrete [5,6] and recycled aggregate concrete [7], have also been introduced into circular CFSST stub columns, with their distinct structural performance and resistances experimentally studied, while the behaviour and resistances of circular CFSST stub columns with novel spiral-welded stainless steel tubes were investigated by Gunawardena and Aslani [8] based on tests. At member level, Uy et al. [3] and

* Corresponding author.

E-mail address: ou.zhao@ntu.edu.sg (O. Zhao).



Fig. 3. Experimental setup for initial global geometric imperfection measurements.

measured longitudinal strains at the two extreme fibres of the stainless steel tube consist of two components: (i) strains resulting from the compression load $\varepsilon_c = (\varepsilon_{\max} + \varepsilon_{\min})/2$ and (ii) strains resulting from the bending moment (due to the initial loading eccentricity, initial mid-height global geometric imperfection and mid-height lateral deflection) $\varepsilon_b = (\varepsilon_{\max} - \varepsilon_{\min})/2$, where ε_{\max} and ε_{\min} are respectively the maximum and minimum longitudinal strains measured from the two strain gauges at the extreme fibres. The corresponding curvature at the mid-height of the column specimen κ can then be calculated as $\kappa = \varepsilon_b/0.5D$, with the corresponding mid-height bending moment given as $M = (EI)_h\kappa$, where

$(EI)_h = EI + E_{cm}I_c$ is the flexural stiffness, where E_{cm} and E are the elastic moduli of the inner concrete and outer stainless steel tube, respectively, while I_c and I are the second moments of area of the inner concrete and outer stainless steel tube, respectively. The sum of the initial loading eccentricity and initial mid-height global geometric imperfection magnitude is then given as the mid-height bending moment divided by the compression load minus the mid-height lateral deflection, with the final expression shown by Eq. (1), where N is the applied compression load and Δ is the mid-height lateral deflection measured from the LVDT. Note that Eq. (1) was derived based on an assumption that the structural behaviour was close to linear elastic (i.e. allowing for linear superposition of strains resulting from compression load and bending moment), and thus a small preload approximately equal to 10% of the expected failure load was applied onto the column specimen and used to calculate the sum of the initial loading eccentricity and initial mid-height global geometric imperfection magnitude. If the calculated $(\omega_g + e_0)$ was greater than $L_e/1000$, the position of the column specimen was re-adjusted, with the preloading procedures repeated, until the achievement of $(\omega_g + e_0) < L_e/1000$ [26,27]. Upon completion of the alignment of the column specimen, a constant loading rate of 0.3 mm/min was adopted until the specimen failed.

$$\omega_0 + \omega_g = \frac{(EI)_h(\varepsilon_{\max} - \varepsilon_{\min})}{DN} - \Delta \quad (1)$$

The measured load-mid-height lateral deflection curves of the four series of circular HCFST column specimens are depicted in Fig. 5(a)–(d), respectively. The key obtained test results, including the actual combined initial global geometric imperfection magnitude and initial loading eccentricity $(\omega_g + e_0)$, the failure load N_u , the mid-height lateral deflection at the failure load Δ_u , and the reduction factor for flexural buckling χ , given as the ratio of the failure load to the sum of the plastic resistances of the inner concrete and outer stainless steel tube (i.e. $\chi = N_u/(A_c f_c + A_s \sigma_{0.2})$, where A_c and A_s are the cross-section areas of the inner concrete and outer stainless steel tube, respectively), are presented in Table 4. All the circular HCFST column specimens were found to fail by flexural buckling, with the deformed failure

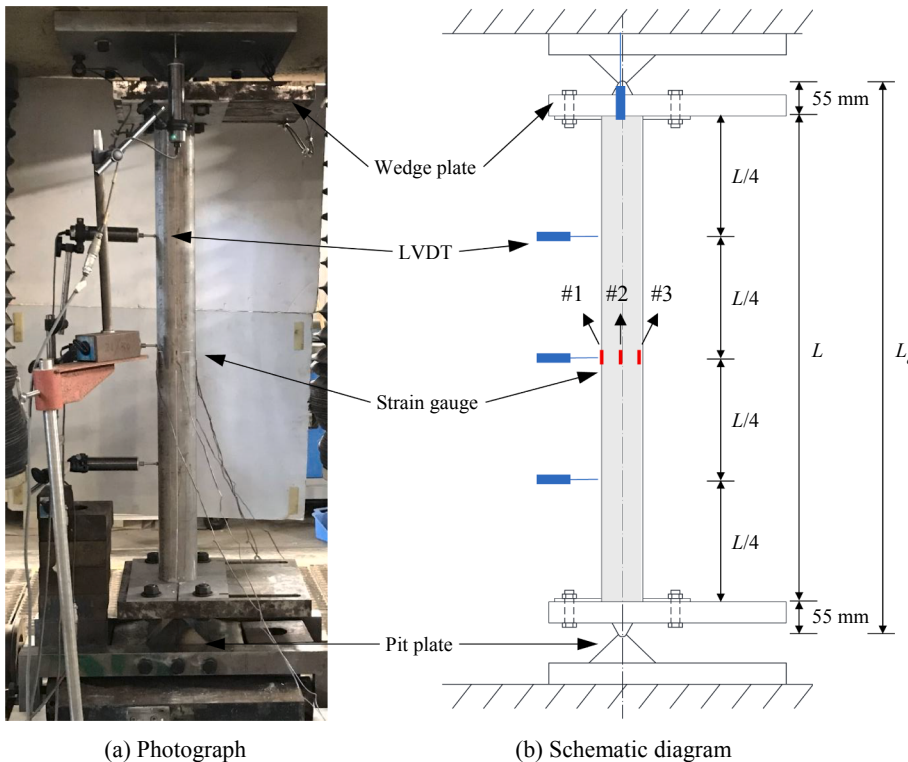


Fig. 4. Pin-ended column test setup.

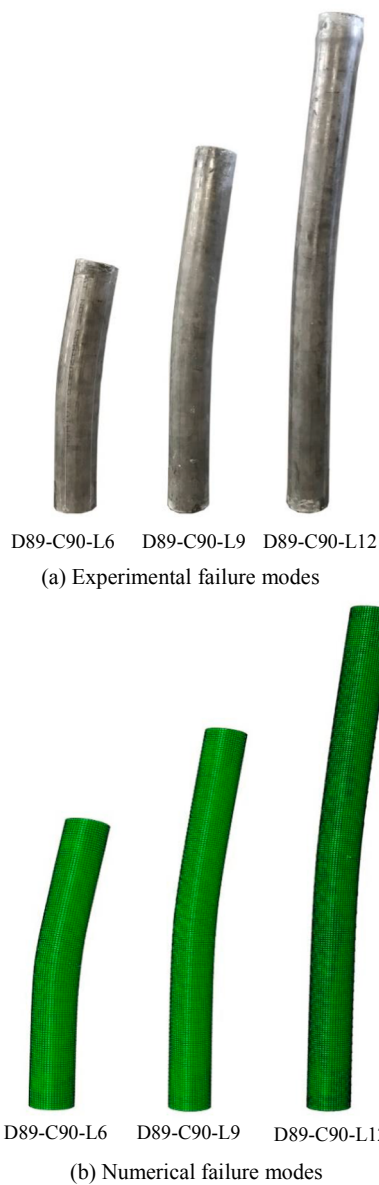


Fig. 6. Experimental and numerical failure modes for a typical specimen series D89-C90.

$$\bar{\lambda}_{EC4} = \sqrt{\frac{N_{pl,Rk}}{N_{cr}}} \quad (2)$$

$$N_{cr} = \frac{\pi^2(EI)_{eff,EC4}}{L_e^2} \quad (3)$$

$$(EI)_{eff,EC4} = EI + 0.6E_{cm}I_c \quad (4)$$

2.5.2. Reduction factor for flexural buckling

The influences of the member lengths, stainless steel tube sizes and high strength concrete grades on the flexural buckling resistances of circular HCFST columns are examined herein. For each specimen series, the experimentally obtained reduction factors for flexural buckling χ are plotted against the corresponding member relative slendernesses $\bar{\lambda}_{EC4}$ and shown in Fig. 8. It can be observed that the flexural buckling reduction factors χ are generally greater than 1.0 for circular HCFST columns with $\bar{\lambda}_{EC4}$ less than around 0.5–0.6, indicating that the reductions in cross-section plastic resistances due to global instability (flexural buckling) are not pronounced for circular HCFST

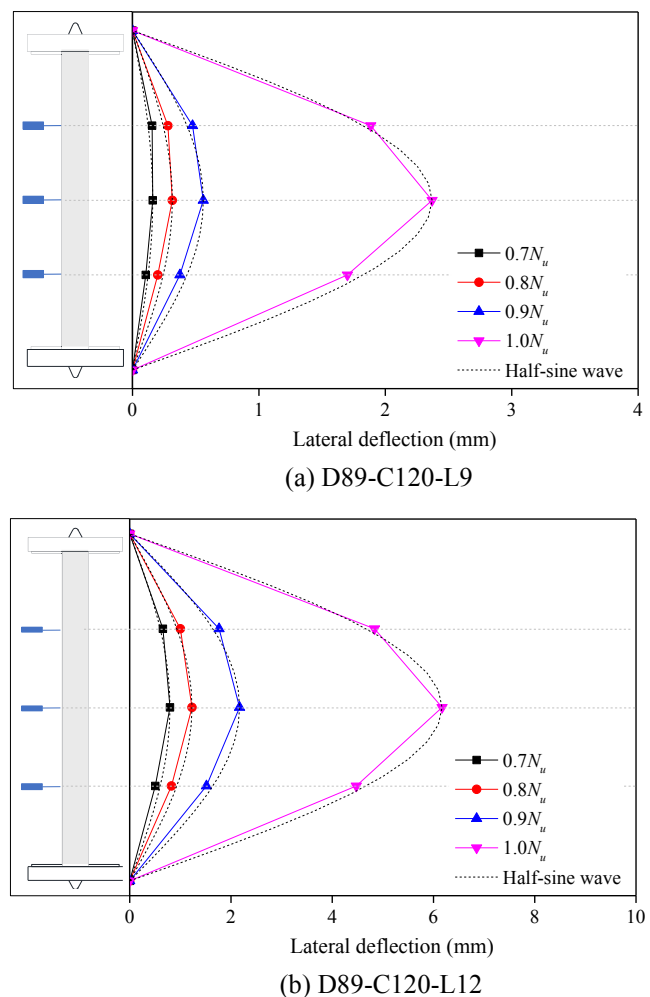


Fig. 7. Lateral deflection distributions for circular HCFST column specimens D89-C120-L9 and D89-C120-L12.

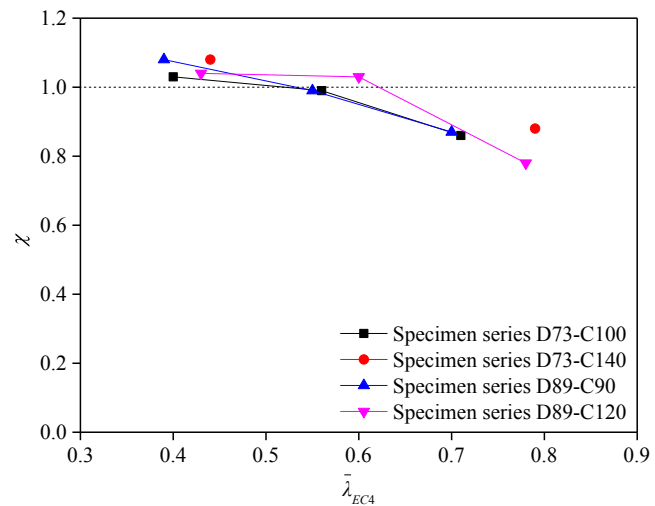


Fig. 8. Flexural buckling reduction factors for circular HCFST column specimens.

columns in the relatively low and intermediate range of member relative slenderness, while the flexural buckling reduction factors χ are less than 1.0 for circular HCFST columns with $\bar{\lambda}_{EC4}$ greater than 0.6, revealing that the detrimental effect of global instability (flexural buckling) on the resistances of circular HCFST columns in the

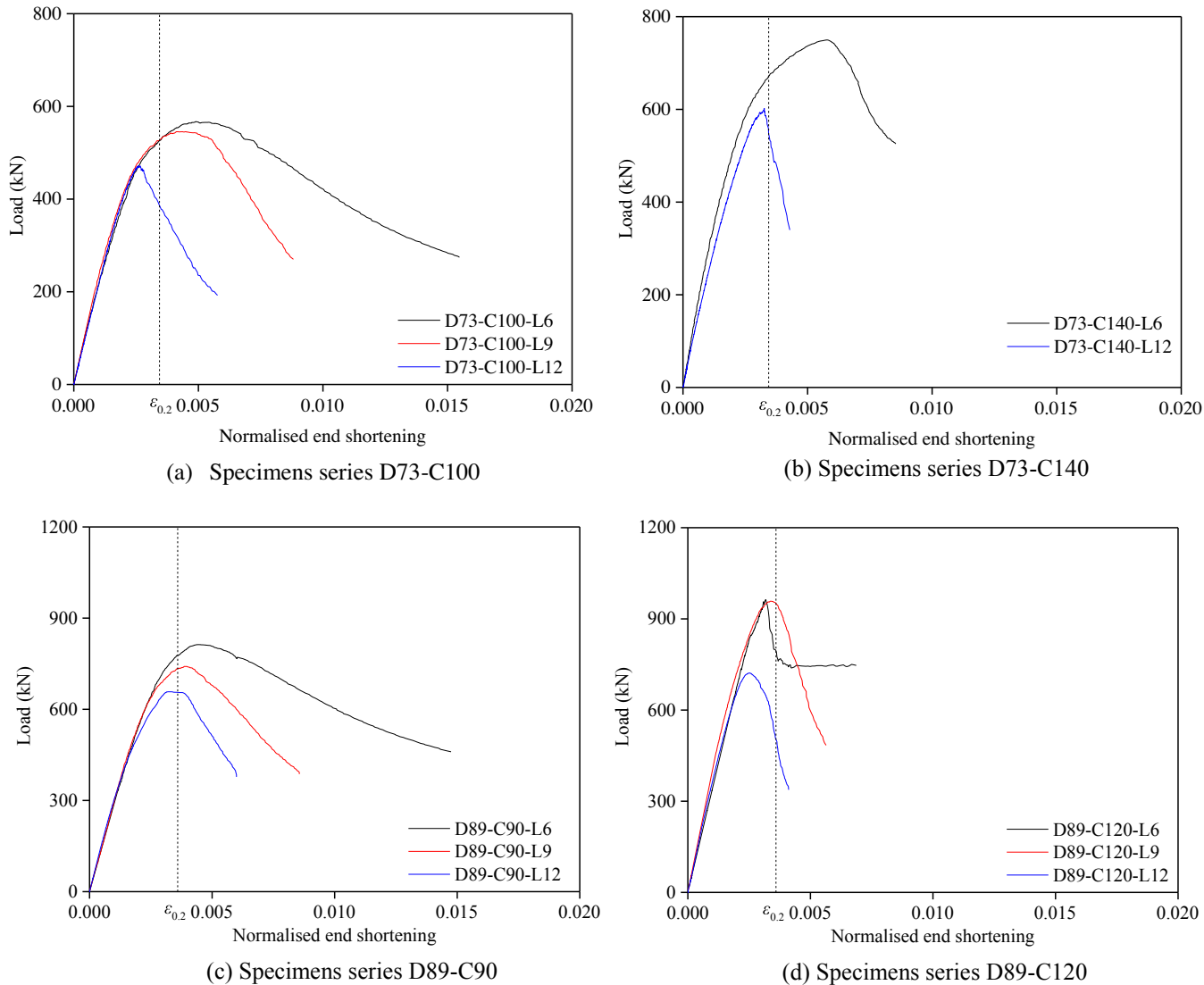


Fig. 9. Load-normalised end shortening curves for circular HCFST column specimens.

relatively high range of member relative slenderness is now obvious and should be allowed for in the design. Moreover, the $\chi-\bar{\lambda}_{EC4}$ curves do not exhibit significant differences among the four series of circular HCFST column specimens, which indicates that the reduction factors for flexural buckling χ are relatively insensitive to the high strength concrete grades and stainless steel tube sizes.

2.5.3. Load-end shortening response

The load-strain ($N-\delta/L$) curves, converted from the measured load-end shortening ($N-\delta$) curves through dividing the end shortenings by the member lengths, are presented in Fig. 9(a)-(d), where the yield strains corresponding to the material yield (0.2% proof) stresses of the stainless steel tubes $\epsilon_{0.2}$, as measured from material testing, are also shown. It can be seen from Fig. 9(a)-(d) that the $N-\delta/L$ curves of the circular HCFST column specimens within each series are almost identical during the early stage of loading but different for higher compression loads. Moreover, the column specimens with longer member lengths were shown to fail earlier (i.e. the strains corresponding to the failure loads are smaller) than their shorter counterparts, owing to the higher detrimental effects from global instability. It is also worth noting that the strains at the failure loads for those relative long column specimens are smaller than the corresponding yield strains of the stainless steel tubes, as evident in Fig. 9(a)-9(d), indicating that

the average failure stresses of the stainless steel tubes are less than the material 0.2% proof stresses due to the influence from global instability.

2.5.4. Longitudinal strains of stainless steel tube

The development of the longitudinal strains of stainless steel tubes are discussed in this section. The load-longitudinal strain curves, recorded by the three strain gauges (#1, #2 and #3 - Fig. 4) attached to the column mid-height, for a typical specimen D89-C120-L9, are depicted in Fig. 10, while the corresponding strains at the extreme fibres (measured from the strain gauges #1 and #3) and the mid-point of the extreme fibres (measured from the strain gauge #2) of the stainless steel tube at five load levels – $0.2N_u$, $0.4N_u$, $0.6N_u$, $0.8N_u$ and N_u are displayed in Fig. 11. It is evident in Fig. 10 and Fig. 11 that the longitudinal strains at the three measured positions are different upon loading, owing to the existence of initial global geometric imperfection and initial loading eccentricity (and thus bending moment at the specimen mid-height). Moreover, the discrepancy of the longitudinal strains measured from the three strain gauges was found to increase with the applied compression load, due to the increasing effect of bending moment resulted from the growing mid-height lateral deflection. The whole cross-section of the stainless steel tube at mid-height was in compression when the peak load was reached, but part of the

